

Fast LIBS Identification of Aluminum Alloys

Walid Tawfik Y. Mohamed

*National Inst. of Laser Enhanced Science NILES, Dept. of Environmental Applications, Cairo University, Cairo, Egypt
Faculty of Education for Girls, Department of Physics, Gurayyat, North of Al-gouf, Kingdom of Saudi Arabia*

E-mail: Walid_Tawfik@hotmail.com

Laser-induced breakdown spectroscopy (LIBS) has been applied to analysis aluminum alloy targets. The plasma is generated by focusing a 300 mJ pulsed Nd: YAG laser on the target in air at atmospheric pressure. Such plasma emission spectrum was collected using a one-meter length wide band fused-silica optical fiber connected to a portable Echelle spectrometer with intensified CCD camera. Spectroscopic analysis of plasma evolution of laser produced plasmas has been characterized in terms of their spectra, electron density and electron temperature assuming the LTE and optically thin plasma conditions. The LIBS spectrum was optimized for high S/N ratio especially for trace elements. The electron temperature and density were determined using the emission intensity and Stark broadening, respectively, of selected aluminum spectral lines. The values of these parameters were found to change with the aluminum alloy matrix, i.e. they could be used as a fingerprint character to distinguish between different aluminum alloy matrices using only one major element (aluminum) without needing to analysis the rest of elements in the matrix. Moreover, It was found that the values of T_e and N_e decrease with increasing the trace elements concentrations in the aluminum alloy samples. The obtained results indicate that it is possible to improve the exploitation of LIBS in the remote on-line industrial monitoring application, by following up only the values of T_e and N_e for aluminum in aluminum alloys as a marker for the correct alloying using an optical fiber probe.

1 Introduction

The interaction of high-power pulsed laser light with a target or solid samples has been an active topic not only in plasma physics but also in the field of analytical chemistry. During the past decade, the use of Laser Induced Plasma Spectroscopy (LIBS) as an alternative elemental analysis technology based on the optical emission spectra of the plasma produced by the interaction of high-power laser with a target has been studied by several authors [1–7]. Because of the lack of pre-treatment of the material as well as the speed of analysis, not mentioning the possibility of in situ analysis, this technique offers an attractive solution for a wide range of industrial applications. However, the existent commercial instruments are still not sufficient to guarantee reproducibility and precise quantitative results. In fact, the analytical performance of the LIBS technique depends strongly on the choice of experimental conditions that influence the laser-produced plasma characteristics [8]. The main parameters affecting the performance of LIBS results are as follows: laser intensity, excitation wavelength, laser pulse duration, and the surrounding atmosphere [9]. Moreover, the physical and chemical properties of the sample can affect the produced plasma composition, a phenomenon known as the matrix effect. The interaction between the laser and the target in LIBS is influenced significantly by the overall composition of the target, so that the intensity of the emission lines observed is a function

of both the concentration of the elements of interest and the properties of the matrix that contains them. The author published works studied the matrix effect under different experimental conditions to specify causes and find out the methods of correction [4, 6, 7].

On the other hand, from a more fundamental point of view, LIBS diagnostic studies of electron temperature T_e and number density N_e have all been based on assumptions, most importantly those of the existence of local thermodynamic equilibrium LTE conditions and of optically thin plasma [10]. Ciucci et al. [11] have discussed the possibility of devising a calibration free method, i.e. some kind of an “absolute analysis” approach. The success of such approach heavily relies upon the accurate knowledge of the parameters and the validity of the assumptions cited above. Apparently LIBS plasmas fulfill LTE conditions even though during the measurement time, the plasma parameters rapidly change due to expansion. In this connection, one needs to determine the conditions for expanding high density plasmas to be in an equilibrium state as well as of the time duration for the existence of such equilibrium. The aim of the present paper is to study the variation of the plasma parameters with aluminum lines in different aluminum alloy matrices. This will help not only clarifying the constraints to be taken into account when measuring T_e and N_e but also using the matrix effect to distinguish different aluminum alloy matrices.

Sample	Be	Mg	Si	Fe	Cu	Ca	Mn	Al
AL 6063	0.00030	0.54	0.43	0.2	0.085	0.0021	0.081	Balance
AL 4104	0.0017	1.56	9.63	0.7	0.12	0.0021	0.046	Balance
AL 5754	0.0022	2.54	0.22	0.35	0.1	0.0011	0.29	Balance
AL 3104	0.0011	1.15	0.21	0.42	0.17	0.0031	0.92	Balance

Table 1: Beryllium, Copper, iron, magnesium, silicon, calcium and manganese concentrations (in w/w %) in the standard aluminum alloy samples.

2 Experimental setup

A typical LIBS experimental setup, described in details by the author elsewhere [4, 6], is used throughout the present investigations. The plasma formation was attained with the aid of a Q-switched Nd: YAG laser (NY81.30, continuum, USA) operating at 1064 nm (pulse duration of 7 ns) and repetition rate of 0.1 Hz–30 Hz. The laser pulse energy of 100–300 mJ was adjusted by a suitable combination of beam splitters at constant operating high voltage (1.3 kV) and Q-switch delay (1.65 μ s) to ensure spatial and temporal beam profile stability. An energy meter (Nova 978, Ophir Optonics Ltd., USA) was employed to monitor the shot to shot pulse energy. The laser beam was focused on aluminum alloy samples by a 10 cm focal length quartz lens to generate the plasma. The emitted light from the plasma plume is collected via a one-meter length wide band fused-silica optical fiber connected to a 0.17 m focal length Echelle spectrometer (Mechelle 7500, Multichannel Instruments, Sweden). The Mechelle 7500 provides a constant spectral resolution of 7500 corresponding to 4 pixels FWHM, over a wavelength range 200–1000 nm displayable in a single spectrum. A gateable, intensified CCD camera, (DiCAM-Pro, PCO Computer Optics, Germany) coupled to the spectrometer was used for detection of the dispersed light. The overall linear dispersion of the spectrometer-camera system ranges from 0.006 nm/pixel (at 200 nm) to 0.033 nm/pixel (at 1000 nm). To avoid the electronic interference and jitters, the CCD intensifier high voltage was triggered optically. The ICCD camera control was performed via Mechelle software (Multichannel Instruments, Stockholm, Sweden). The emission spectra display, processing and analysis were done using 2D- and 3D-GRAMS/32 version 5.1 spectroscopic data analysis software (Galactic Industries, Salem, NH, USA). To improve data reproducibility, and to avoid electronic jittering problem, the laser was set to single shot mode. Then, the Nd:YAG laser beam was focused onto the sample surface at 90° angle. This was done using a 25 mm diameter dichroic mirror that reflects 99% of high energy 1064 nm wavelength. The focal point was set 5 mm below the surface of the sample in order to generate plasma of 800 μ m spot diameter. This also minimize breakdown above the surface of any particles and aerosols generally present above the sample. Moreover, for each new sample, before spectral collection, 20 laser pulses were performed to clean the sample surface and removes

surface oxides and contamination to ensure that the observed spectrum is representative of the sample composition.

On the other hand, the use of a micro *xyz*-translation stage as a holder for fused-silica optical fiber facilities maximum intensity of the observed emission light from the plasma plume. Now, we aim to produce LIBS spectra with high precision. Precision is the measure of the degree of reproducibility of a measurement. Laser shot-to-shot variation causes differences in the plasma properties, therefore affects the magnitude of the element signal, and hence degrades the LIBS precision. To improve LIBS precision, spectra from several laser shots have to be averaged in order to reduce statistical error due to laser shot-to-shot fluctuation. We reproduced the measurements at five locations on the sample surface in order to avoid problems linked to sample heterogeneity. Twenty shots were fired at each location and saved in separated files and the average was computed and saved to serve as the library spectrum. For each recorded spectrum, the peak intensity, the Lorentzian curve fitting, the full width at half maximum FWHM, and the center wavelength of each line, as well as the background emission continuum are determined. Data treatment preprocessing of the averaged spectra data was performed in the Windows environment on a Pentium 4 PC using GRAMS/32, Excel (Microsoft Office Excel 2003) and Origin software version 7.0220 (Origin Lab Corp., USA). The averages of peak tables (lists of wavelengths and intensities) of the averaged spectra were roll generated in GRAMS/32 and exported for data evaluation.

We investigated a set of five standard samples of aluminum alloy to study the dependence of the electron density and temperature on the matrix effect. So that, these samples were selected to have trace elements with a range of concentrations. We used disk shaped standard samples of aluminum alloy provided by Alcan international limited (0.5 cm; $\phi = 5$ cm). The concentrations of the trace elements “Mg, Si, Be, Cu, Mn, Fe, Ca” in the aluminum alloy samples are given in Table 1.

3 Results and discussion

3.1 Optimizing LIBS spectrum

Optimizing LIBS for a high resolution aluminum alloy was done by optimizing the experimental conditions including the time delay, the gate delay (the integration time) and the laser irradiance. In fact, the timing of the recorded signal

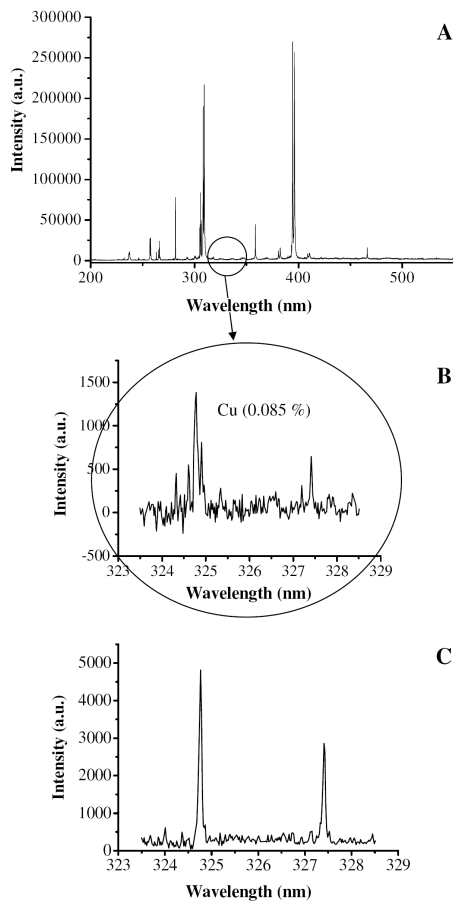


Fig. 1: The figure contains three spectra as follows: A — the panoramic LIBS spectrum in the spectral range 200–700 nm shows the UV-visible emission lines of aluminum as a major element and the emission lines of the trace elements in the aluminum alloy sample AL 6063. B — a zoomed segment showing the copper lines 324.7 nm and 327.4 nm in the UV region recorded at 1.5 μs delay time and 1 μs gate width using laser irradiance of 10^8 W/cm^2 for sample AL 6063 containing copper concentration of 0.085% (w/w) where $S/N = 8$. C — the same copper lines using the optimized conditions of 2.5 μs delay time and 1.5 μs gate width at 10^{10} W/cm^2 laser irradiance where $S/N = 25$.

depend on the laser energy and wavelength, so we firstly increased the laser energy from 70 mJ, as used before by the author [6], to 300 mJ. In this case, the laser irradiance increased from $\approx 10^8 \text{ W/cm}^2$ to $\approx 10^{10} \text{ W/cm}^2$ which found to be suitable for the case of aluminum alloy samples having trace elements with concentrations in the ppm range. Then under the late laser irradiance, the delay time, at which the spectrum is recorded from the laser start, was optimized by scanning the delay time with the signal intensity as done previously by the author [6]. It was found that the optimized conditions are 2.5 μs delay time and 1.5 μs gate width at 10^{10} W/cm^2 laser irradiance at the sample surface. The gate delay was limited to 1.5 μs to avoid saturation of the detector. Optimizing LIBS spectrum was done in order to reduce

the background signal and increase the signal to noise ratio (S/N). Figure 1 shows a typical plasma emission spectrum for aluminum alloy sample AL 6063. The figure contains three spectra as follows: A — the panoramic LIBS spectrum in the spectral range 200–700 nm shows the UV-visible emission lines of aluminum as a major element and the emission lines of the trace elements in the aluminum alloy sample. B — a zoomed segment showing the copper lines 324.7 nm and 327.4 nm in the UV region recorded at 1.5 μs delay time and 1 μs gate width using laser irradiance of 10^8 W/cm^2 for sample AL 6063 containing copper concentration of 0.085% (w/w) where $S/N = 8$. C — the same copper lines using the optimized conditions of 2.5 μs delay time and 1.5 μs gate width at 10^{10} W/cm^2 laser irradiance where $S/N = 25$. This, of course, makes LIBS to be a very high-resolution spectroscopic system for the trace elements with concentrations in the ppm range.

3.2 Plasma parameters and matrix effect

The main factors that influence the light emitted by the plasma are its temperature, the number density of the emitting species, and the electronic density. The number density of the emitting species (e.g. atoms, ions, etc) depends on the total mass ablated by the laser, the plasma temperature, and the degree of the excitation and/or ionization of the plasma. The vaporized amount, in turn, depends on the absorption of the incident laser radiation by the surface, the plasma shielding [12], which is related to the electron density of the plasma, and the laser fluence. Therefore, the knowledge of the plasma temperature and the density of plasma species are vital for the understanding of the dissociation–atomization, excitation, and ionization processes occurring in the plasma. For this reason, study the variation of these plasma parameters with aluminum lines in different aluminum alloy matrices. This will help not only clarifying the constraints to be taken into account when measuring T_e and N_e but also using the matrix effect to distinguish different aluminum alloy matrices.

For plasma in local thermodynamic equilibrium (LTE), the population density of atomic and ionic electronic states is described by a Boltzmann distribution. For optically thin plasma, the re-absorption effects of plasma emission are negligible. So, the emitted spectral line intensity I is a measure of the population of the corresponding energy level of this element in the plasma. For the LTE plasma, the population of an excited level can be related to the total density $N(T)$ of neutral atom or ion of this element by Boltzmann equation [13] as:

$$I = \frac{hc}{4\pi\lambda} N(T) \frac{A_{ki} g_k}{U(T)} \exp\left(-\frac{E_k}{KT}\right), \quad (1)$$

where λ is the wavelength, A_{ki} is the transition probability, g_k is the statistical weight for the upper level, E_k is the

Wavelength (nm)	A_{ki} (s^{-1})	E_k (cm^{-1})	g_k	Stark broadening parameter W (nm)
281.62	3.83E+08	95351	1	4.2900E-04
308.85	1.50E+07	139289.2	5	—
364.92	1.50E+07	132823	3	—
364.92	1.50E+07	132823	3	—
365.11	2.10E+07	132822.8	5	—
365.11	2.10E+07	132822.8	5	—
365.50	2.70E+07	132822.9	7	—
365.50	2.70E+07	132822.9	7	—
370.32	3.80E+07	133916.4	5	—
373.20	4.30E+06	132215.5	3	—
373.39	1.30E+07	132215.5	3	—
373.80	2.10E+07	132215.5	3	—
386.62	3.70E+07	132778.6	1	—
390.07	4.80E+05	85481.35	5	—
559.33	1.10E+08	124794.1	5	—
624.34	1.10E+08	121483.5	7	—

Table 2: A list of the spectroscopic data of the aluminum spectral lines used for the determination of plasma temperature and density of aluminum alloy samples.

excited level energy, T is the temperature (in LTE all temperatures are assumed to be equal, i.e. $T_e \approx T_{ion} \approx T_{plasma}$), K is the Boltzmann constants, $U(T)$ is the partition function.

The emitted spectral line intensity from a given state of excitation can be used to evaluate the plasma temperature. The lines must be well resolved for accurately evaluating their wavelengths λ , intensities I , and their transition probabilities A_{ki} must be known.

Reformulating Eqn. (1) gives;

$$\ln \frac{I\lambda}{A_{ki} g_k} = -\frac{1}{KT} E_k + \ln \frac{C F}{U(T)}, \quad (2)$$

where F is an experimental factor and C is the species concentration.

By plotting the left hand side of Eqn. (2) vs. the excited level energy E_k , the plasma temperature can be obtained from the slope of obtained straight line.

During the early stages of plasma formation, the emitted spectrum is dominated by an intense continuum (Bremsstrahlung radiation), on which several heavily broadened ionic lines of the elements present are superimposed. The broadening of the ionic lines is due to the high electron densities occurring at this initial period (Stark broadening). At the same time, the excited neutral atoms' spectral lines are relatively weak; they are superimposed on the continuum and often overlap with the ionic lines. Hence, they cannot be easily isolated and measured. As a consequence, the measurement of their intensity for the construction of Boltzmann plots becomes problematic at early times (e.g. the first few

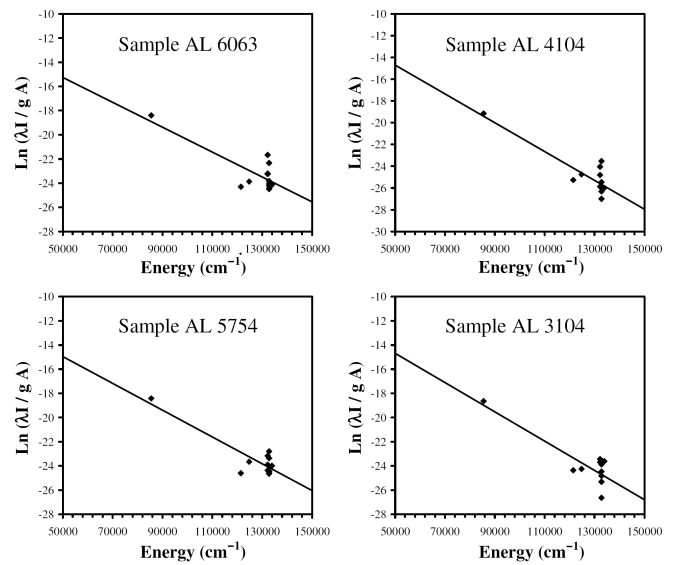


Fig. 2: Four Boltzmann plots were determined from the emission line intensities of aluminum observed in the laser-induced plasma of aluminum alloys. The slope of the plotted curves yields temperatures 13960 K, 12974 K, 11871 K, and 10841 K for the samples AL 6063, AL 5754, AL 3104 and AL 4104 respectively.

hundred nanoseconds) and the use of time delay is compulsory. However, each spectral line exhibits different temporal evolution that is element and atomic energy level specific. Under our experimental conditions, a delay time of $2.5 \mu s$ and $1.5 \mu s$ gate width at $10^{10} W/cm^2$ laser irradiance have been determined as optimum conditions (as described in Section 3.1 before). Under these experimental conditions, the plasma temperatures were determined from the emission line intensities of sixteen selected aluminum lines (see Table 2) observed in the laser-induced plasma of different aluminum alloy targets. Figure 2 shows four Boltzmann plots of Eqn. (2), for these lines where the data were fitted with the least-square approximation. The spectral lines wavelengths, energies of the upper levels, statistical weights, and transition probabilities used for these lines were obtained from NIST [14] and Griem [13], and listed in Table 3. The slope of the plotted curves yields temperatures 13960 K, 12974 K, 11871 K, and 10841 K for the samples AL 6063, AL 5754, AL 3104 and AL 4104 respectively as listed in Table 3).

On the other hand, the electron number density can be obtained from the Stark-broadening of the emission lines [15]. This is because, Stark-broadening results from Coulomb interactions between the radiator and the charged particles present in the plasma. Both ions and electrons induce Stark broadening, but electrons are responsible for the major part because of their higher relative velocities. The electrons in the plasma can perturb the energy levels of the individual ions which broaden the emission lines originating from these excited levels. Stark broadening of well-isolated lines in the

Plasma parameters	Sample AL6063	Sample AL 5754	Sample AL 3104	Sample AL 4104
Electron Temperature (Kelvin)	13960	12974	11871	10841
Electron Density (cm^{-3})	7.28×10^{18}	4.28×10^{18}	4.44×10^{18}	2.28×10^{18}

Table 3: The plasma electron temperature T_e and density N_e determined from aluminum spectral lines in the four standard aluminum alloy samples.

plasma is, thus, useful for estimating the electron number densities provided that the Stark-broadening coefficients have been measured or calculated. The line profile for stark broadened is well described by a Lorentzian function. Since the instrumental line-broadening exhibit Gaussian shape, then the stark line width $\Delta\lambda_{FWHM}$ can be extracted from the measured line width $\Delta\lambda_{observed}$ by subtracting the instrumental line broadening $\Delta\lambda_{instrument}$:

$$\Delta\lambda_{FWHM} = \Delta\lambda_{observed} - \Delta\lambda_{instrument}. \quad (3)$$

In our case $\Delta\lambda_{instrument}$ was 0.05 nm (determined by measuring the FWHM of the Hg lines emitted by a standard low pressure Hg lamp).

The width of stark broadening spectral line depends on the electron density N_e . Both the linear and the quadratic stark effect are encountered in spectroscopy. Only the hydrogen atom and H-like ion exhibit the linear stark effect. For the linear stark effect the electron density should be deduced from H line width from the formula [13]

$$N_e = C(N_e, T) \Delta\lambda_{FWHM}^{3/2} \quad (4)$$

the values of the parameter $C(N_e, T)$ are tabulated in the literature [13], which determine the relative contribution of the electron collision on the electrostatic fields, and depend weakly on N_e and T .

For a non-H-like line, the electron density (in cm^{-3}) could be determined from the FWHM of the line from the formula [13]:

$$N_e \approx \left(\frac{\Delta\lambda_{FWHM}}{2W} \right) \times 10^{16}, \quad (5)$$

W is the electron impact parameter (stark broadening value) and it is given in Table 2). The last formula is generally used for calculations of plasma generated from solid targets [7, 12].

The aluminum line 281.62 nm was identified as candidate for electron-density measurements. Figure 3 shows, the 281.62 nm line with sufficient resolution to measure the full width at half-maximum ($\lambda_{1/2}$) at four different aluminum alloy samples. All the data points were fitted with Lorentzian fitting function using the Origin software to determine ($\lambda_{1/2}$) as shown in Fig. 3 and found to be 0.113 nm, 0.070 nm, 0.092 nm and 0.088 nm for the samples AL6063, AL 4104, AL 5754, and AL 3104 respectively. Substituting the values of $\lambda_{1/2}$ in Eqn. (3) and the corresponding value of stark broadening W (4.29×10^{-4} nm from Griem [13] at plasma temperature of 10000 K) in Eqn. (5) the electron density values of 7.28×10^{18} , 4.28×10^{18} , 4.44×10^{18} , and 2.28×10^{18}

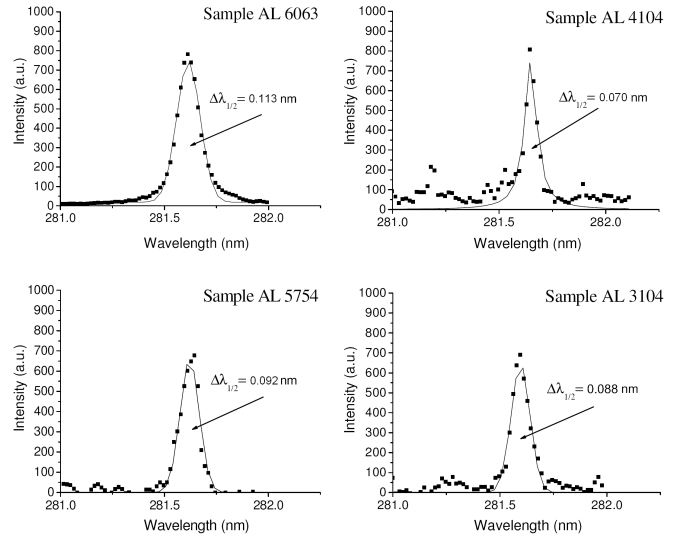


Fig. 3: The 281.62 nm line with sufficient resolution to measure the full width at half-maximum ($\lambda_{1/2}$) at four different aluminum alloy samples. All the data points were fitted with Lorentzian fitting function using the Origin software and the values of $\lambda_{1/2}$ found to be 0.113 nm, 0.070 nm, 0.092 nm and 0.088 nm for the samples AL6063, AL 4104, AL 5754, and AL 3104 respectively.

were obtained for the samples AL 6063, AL 5754, AL 3104 and AL 4104 respectively as listed in Table 3.

The above obtained results reveal that plasma parameters (T_e , N_e) change with changing the aluminum alloy matrix i.e. matrix dependent. Moreover, by comparing the results of the four samples in Table 3 with the concentrations of the trace elements in Table 1, one could recognized that while the concentrations of trace elements increase both values of T_e and N_e decrease. This is well clear by comparing the two samples AL 6063 and AL 4104 thus while all the trace elements, except Mn, increase (silicon concentration increases from 0.43% to 9.63%), both values of T_e and N_e decrease from 13960 K, $7.28 \times 10^{18} \text{cm}^{-3}$ to 10841 K, $2.28 \times 10^{18} \text{cm}^{-3}$, respectively. This result might occur because increasing the “trace element” concentration comprises increasing portion of the laser-target interaction volume of that trace element and decreases the laser-target interaction volume of the major element (aluminum). Moreover, aluminum “the major element” species are easy to be ionized than the species of the seven trace elements which leads to higher electron density for aluminum alloy samples with low trace elements concentrations than for relatively high trace elements concentrations. Moreover, this is clear since,

the ionization potential of Al, Ca, Be, Mg, Si, Mn, Fe, and Cu are (in eV) 5.98, 6.11, 9.32, 7.64, 8.15, 7.43, 7.87 and 7.72 respectively. The last observed result agrees with previously observed results obtained by O. Samek [15] and Rusak et al. [16].

Finally, by knowing the electron density and the plasma temperature we can determine whether the local thermodynamic equilibrium (LTE) assumption is valid applying the criterion given by McWhirter [17], Bekefi [18] where the lower limit for electron density for which the plasma will be in LTE is:

$$N_e \geq 1.4 \times 10^{14} \Delta E^3 T^{1/2}, \quad (6)$$

ΔE is the largest energy transition for which the condition holds and T is the plasma temperature.

In the present case $\Delta E = 4.34$ eV for Mg (see Ref. [13]) and the highest temperature is 1.2 eV (13960 K), then the electron density lower limit value given by Eqn. (6) is $1.25 \times 10^{16} \text{ cm}^{-3}$. The experimentally calculated densities are greater than this value, which is consistent with the assumption that the LTE prevailing in the plasma.

4 Conclusion

LIBS technique has been used to analysis different aluminum alloy samples. The LIBS spectrum was optimized for high S/N ratio especially for trace elements. The characteristic plasma parameters (T_e , N_e) were determined using selected aluminum spectral lines. The values of these parameters were found to change with the aluminum alloy matrix, i.e. they could be used as a fingerprint character to distinguish between different aluminum alloy matrices using only one major element (aluminum) without needing to analysis the rest of elements in the matrix. Moreover, It was found that the values of T_e and N_e decrease with increasing the trace elements concentrations in the aluminum alloy samples.

For industrial application, LIBS could be applied in the on-line industrial process that following up elemental concentration in aluminum alloys by only measuring T_e and N_e for the aluminum using an optical fiber probe. This could be done by building a database containing the determined values of T_e and N_e for a range of standard aluminum alloy matrices. Then the unknown aluminum alloy sample could be identified just by comparing its measured T_e and N_e values with the previously stored values in our database.

Acknowledgment

The author gratefully acknowledges the support of Prof. Mohamed Abel-Harith and Prof. M. Sabsabi specially for offering the aluminum alloy samples.

Submitted on February 07, 2007

Accepted on March 06, 2007

Revised version received on March 15, 2007

References

1. Radziemski L. J. Review of selected analytical applications of laser plasmas and laser ablation, 1987–1994. *Microchem. J.*, 1994, v. 50, 218–234.
2. Rusak D. A., Castle B. C., Smith B. W., and Winefordner J. D. Fundamentals and applications of laser-induced breakdown spectroscopy. *Crit. Rev. Anal. Chem.*, 1997, v. 27, 257–290.
3. Radziemski L. From LASER to LIBS, the path of technology development. *Spectrochim. Acta B*, 2002, v. 57, 1109–1113.
4. Sabsabi M., Detalle V., Harith M. A., Walid Tawfik and Imam H. Comparative study of two new commercial Echelle spectrometers equipped with intensified CCD for analysis of laser-induced breakdown spectroscopy. *Applied Optics*, 2003, v. 42, No. 30, 6094–6098.
5. Soliman M., Walid Tawfik and Harith M. A. Quantitative elemental analysis of agricultural drainage water using laser induced breakdown spectroscopy. *First Cairo Conference on Plasma Physics & Applications*, 2003, Cairo, Egypt, Forschungszentrum Juelich GmbH, Bilateral Seminars of the International Bureau, v. 34, 240–243.
6. Ismail M. A., Imam H., Elhassan A., Walid Tawfik and Harith M. A. LIBS limit of detection and plasma parameters of some elements in two different metallic matrices. *J. Anal. At. Spectrom.*, 2004, v. 19, 1–7.
7. Walid Tawfik and Abeer Askar. Study of the matrix effect on the plasma characterization of heavy elements in soil sediments using LIBS with a portable Echelle spectrometer. *Progress in Physics*, 2007, v. 1, 47–53.
8. Castle B., Talabardon K., Smith B. W. and Winefordner J. D. *Appl. Spectrosc.*, 1998, v. 52, 649–657.
9. Tognoni E., Palleschi V., Corsi M. and Cristoforetti G. *Spectrochim. Acta Part B*, 2002, v. 57, 1115–1130.
10. Yalcin S., Crosley D. R., Smith G. P. and Faris G. W. *Appl. Phys. B*, 1999, v. 68, 121–130.
11. Ciucci A., Corsi M., Palleschi V., Rastelli S., Salvetti A. and Tognoni E. *Applied Spectroscopy*, 1999, v. 53, 960–964.
12. Le Drogoff B., Margot B., Chakera M., Sabsabi M., Barthelmy O., Johnstona T. W., Lavillea S., Vidala F. and von Kaenela Y. *Spectrochimica Acta Part B*, 2001, v. 56, 987–1002.
13. Griem H. R. *Plasma Spectroscopy*. McGraw-Hill, N.Y., 1964.
14. NIST National Institute of Standards and Technology, USA, electronic database, http://physics.nist.gov/PhysRefData/ASD/lines_form.html
15. Samek O., Beddows D. C. S., Telle H. H., Kaiser J., Liska M., Caceres J. O. and Gonzales Urena A. *Spectrochimica Acta Part B*, 2001, v. 56, 865–875.
16. Rusak D. A., Clara M., Austin E. E., Visser K., Niessner R., Smith B. W. and Winefordner J. D. *Applied Spectroscopy*, 1997, v. 51, No. 11, 1628–1631.
17. McWhirter R. W. P. In: *Plasma Diagnostic Techniques*, Academic Press, New York, 1965, Ch. 5, 206.
18. Bekefi G. *Principles of laser plasmas*. Wiley, New York, 1976, 550–605.